University of Groningen

The Pericytic Phenotype of Adipose Tissue-Derived Stromal Cells Is Promoted by NOTCH2

Terlizzi, Vincenzo; Kolibabka, Matthias; Burgess, Janette; Hammes, Hans Peter; Harmsen, Martin

IMPORTANT NOTE: You are advised to consult the publisher's version (publisher's PDF) if you wish to cite from it. Please check the document version below.

Document Version
Publisher's PDF, also known as Version of record

Link to publication in University of Groningen/UMCG research database

The Pericytic Phenotype of Adipose Tissue-Derived Stromal Cells Is Promoted by NOTCH2

VINCENZO TERLIZZI [ID],[a,b,c] MATTHIAS KOLIBABKA,[b] JANETTE KAY BURGESS,[c,d] HANS PETER HAMMES,[b] MARTIN CONRAD HARMSEN[a,c]

[a]Lab for Cardiovascular Regenerative Medicine (CAVAREM), Department of Pathology and Medical Biology, [c]Research Institute W.J.Kolff, and [d]Department of Pathology and Medical Biology, GRIAC Research Institute, University Medical Center Groningen, University of Groningen, Groningen, The Netherlands; [b]5th Medical Department, Section of Endocrinology, Medical Faculty Mannheim, University of Heidelberg, Germany

Correspondence: Vincenzo Terlizzi, M.S., Lab for Cardiovascular Regenerative Medicine (CAVAREM), Department of Pathology and Medical Biology, University Medical Center Groningen, University of Groningen, Hanzeplein 1–EA11, Groningen 9713 GZ, The Netherlands. Telephone: +31626711179; e-mail: v.terlizzi@outlook.com

ABSTRACT

Long-term diabetes leads to macrovascular and microvascular complication. In diabetic retinopathy (DR), persistent hyperglycemia causes permanent loss of retinal pericytes and aberrant proliferation of microvascular endothelial cells (ECs). Adipose tissue-derived stromal cells (ASCs) may serve to functionally replace retinal pericytes and normalize retinal microvasculature during disease progression. We hypothesized that Notch signaling in ASC underlies regulation and stabilization of dysfunctional retinal microvascular networks such as in DR. ASC prominently and constitutively expressed NOTCH2. Genetic knockdown of *NOTCH2* in ASC (SH-NOTCH2) disturbed the formation of vascular networks of human umbilical cord vein endothelial cells both on monolayers of ASC and in organotypical three-dimensional cocultures with ASC. On ASC SH-NOTCH2, cell surface platelet-derived growth factor receptor beta was downregulated which disrupted their migration toward the chemoattractant platelet-derived growth factor beta subunits (PDGF-BB) as well as to conditioned media from EC and bovine retinal EC. This chemoattractant is secreted by pro-angiogenic EC in newly formed microvascular networks to attract pericytes. Intravitreal injected ASC SH-NOTCH2 in oxygen-induced retinopathy mouse eyes did not engraft in the preexisting retinal microvasculature. However, the in vivo pro-angiogenic capacity of ASC SH-NOTCH2 did not differ from controls. In this respect, multifocal electroretinography displayed similar b-wave amplitudes in the avascular zones when either wild type ASC or SH-NOTCH2 ASC were injected. In conclusion, our results indicate that NOTCH2 is essential to support in vitro vasculogenesis via juxtacrine interactions. In contrast, ongoing in vivo angiogenesis is influenced by paracrine signaling of ASC, irrespective of Notch signaling. STEM CELLS 2018;36:240–251

SIGNIFICANCE STATEMENT

In this study, NOTCH2 is identified as a novel regulator of pericytic phenotype of human adipose tissue-derived stromal cells (ASCs). Results show that NOTCH2 modulates (a) ASC migration to the retinal microenvironment and (b) endothelial cells assembly in a vessel network formation in vitro. At the molecular level, NOTCH2 promotes the ASC pericytic phenotype through platelet-derived growth factor receptor beta expression and sensitivity to chemoattractant.

INTRODUCTION

Patients affected by diabetes are at risk for developing microvascular complications due to dysregulated glucose metabolism. One of these complications, namely diabetic retinopathy (DR), weakens the capillaries in the eyes leading to blindness [1]. At the cellular level, hyperglycemia (HG) compromises the juxtacrine interactions between pericytes and microvascular endothelial cells (EC) which constitute the retinal capillary network [2]. This is followed by a hypoxia-driven pro-angiogenic response that causes an increase in retinal dysfunctional capillaries that lack pericytic coverage. In normal physiology pericytes wrap around EC, which results in juxtacrine and paracrine cross-communication between the cells that establishes the endothelial barrier and serves to maintain endothelial function [3, 4]. Retinal capillaries have the highest pericytes density in the body; each EC is supported by one pericyte which emphasizes the importance of pericytes in the retina. Migration, differentiation, and stabilization of EC all highly depend on interactions with pericytes.

Stem cell therapy has been exploited for replacement of compromised or lost tissue cells for several decades. Among these therapeutically relevant cells mesenchymal stem cells (MSC), such as adipose tissue-derived stromal/stem cells (ASC) [5], have a strong

potency to differentiate into smooth muscle cells and peri-cytes [6, 7]. Besides this constructive role, ASC are instructive in regenerative processes and secrete a host of mediators that favor the formation and maintenance of blood vessels, that is, vascular endothelial growth factor (VEGF), platelet-derived growth factor (PDGF), angiopoetins-1 and 2 (Ang-1, Ang-2) [8–10]. Moreover, ASC promote remodeling of the extracellular matrix [11, 12], which is essential during vasculo-genesis. Less well-known is that ASC act in a juxtacrine man-ner, that is, engaging in cell-to-cell contact with target cells to influence their function. In vitro, ASC monolayers induce vas-cular(-like) network formation (VNF) of EC, thereby creating a relevant model for investigating the responsible juxtacrine mediators on ASC [13]. ASC cultured in vitro phenotypically resemble pericytes and can replace lost pericytes in rodent models of experimental DR [14]. Importantly, we recently showed that ASC are resilient to HG in VNF of EC, suggesting that ASC may be promising for early stage treatment of DR [15].

An important family of proteins involved in vascular mor-phogenesis and maintenance is the Notch family [16]. Mam-mals express four Notch receptors (NOTCH1 to 4) and five membrane bound ligands (JAGGED 1–2 and Delta-like 1–3 and 4). After binding to their ligands, Notch receptors are proteo-lytically activated by a complex of tumor necrosis factor-beta-converting enzyme (ACE) and gamma-secretase. This releases the Notch intracellular domain (NICD) which translocates into the nucleus and binds to C-promoter-binding factor (CBF-1/RBPJk/Su[H]/Lag-1) and coactivator Mastermind-like (MAML) and activates the transcription of downstream genes in partic-ular HEY and HES [17–19]. Furthermore, NICD has been shown to form complex with endothelial transcription factor (ERG) and β-catenin, mediating in turn Ang1-dependent delta-like 4 (Dll4)/Notch signaling in EC [20]. The role of Notch signaling in vascular stability is enhanced by supporting neighboring cells. For example, activation of smooth muscle genes in bona fide pericytes, requires interaction with EC by binding of cell surface NOTCH3 and JAGGED1 [21, 22]. Capillary branching, differentiation, and patterning processes in the retina depend on equilibrium between Notch ligands and receptors on adja-cent cells. Indeed, JAGGED1 is a potent proangiogenic factor which antagonizes Dll4/Notch signaling on EC during sprouting angiogenesis. Pericyte recruitment and JAGGED1 expression results in NOTCH1 upregulation, suppression of tip cells' DLL4 and reduced stalk cells responsiveness to VEGF-A, ultimately leading to homeostasis of the capillaries bed [23, 24]. Besides, Notch signaling activation reduces the volume of age-related macular degeneration [25]. The latter study highlights the role of Notch signaling in maintaining the balance between proan-giogenic genes such as VEGF Receptor 2 (VEGFR2), C-C che-mokine receptor 3 (CCR3) and PDGF-BB and antiangiogenic genes such as VEGFR1 and UNC5B.

Much of the action of ASC is achieved by paracrine sig-naling, yet pericytes and EC also communicate via juxtacrine signaling. We argued that given the differences in sensitivity to HG between ASC and bona fide pericytes, juxtacrine sig-naling will differ too. The current study aims at understand-ing the role of Notch signaling in the pericytic function of ASC in vitro and, in a mouse model of pathological vasoproliferation.

MATERIALS AND METHODS

Primary Cell Cultures and Isolation

ASC were isolated from lipoaspirates as described previously [26]. Anonymously donated samples were obtained with informed consent as approved by the ethical board of the University Medical Center Groningen following the guidelines for "waste materials." Propagation of ASC was in Dulbecco's modified eagle's medium (DMEM) (BioWhittaker, Walkersville, MD): 10% bovine serum albumin (BSA), 1% l-Glutamine, 1% Penicillin/Streptomycin (P/S); which was changed for EC medium (ECM, roswell park memorial institute (RPMI)-1640 (Lonza Biowhittaker Verviers, Belgium), 10% heat inactivated FBS (Thermo Scientific, Hemel Hempstead, U.K.), 100 U/ml penicillin, 100 mg/ml streptomycin (Invitrogen, Carlsbad, CA), 2 mM L-glutamine (Lonza Biowhittaker Verviers, Belgium), 5 U/ml heparin (Leo Pharma, The Netherlands), and 5 μg/ml of EC growth factor) prior to coculture experiments. Human umbilical cord vein endothelial cells (HUVEC) were obtained from Lonza (Breda, The Netherlands) and the Endothelial Cell Facility of University Medical Center Groningen, The Nether-lands. ASC and HUVEC were seeded at $4 \times 10^4/cm^2$. HUVEC were cultured on gelatin-coated tissue culture polystyrene. Bovine retinal endothelial cells (BREC) were isolated from reti-nas of bovine eyes purchased at the local slaughter house [27]. Upon receipt the eyes were briefly immersed in 70% ethanol for sterilization purposes. The retinas were harvested from the eyes (approximately 80 eyes per isolation) and washed in DMEM. Subsequently, the retinas were minced in small pieces and incubated with an enzyme cocktail: collage-nase type 4 (500 μg/ml, Thermo Fisher Scientific, MA), DNase (200 μg/ml, Roche Diagnostic, Mannheim, Germany) and, pro-nase E (200 μg/ml, Roche Diagnostic, Mannheim, Germany) at 37°C for 30 minutes. The digested retinas were filtered through a 53 μm mesh nylon filter and the cell homogenate seeded on gelatin coated plates in DMEM (BioWhittaker, Wal-kersville, MD): 10% FBS, 1% l-Glutamine, 1% Penicillin/Strepto-mycin (P/S). Cells' medium was refreshed every 3 days. ASC and HUVEC were used between passage 3 and 5. BREC pas-saged twice were used for downstream applications.

Gene Transcript Analysis

The gene expression profiles of Notch members were ana-lyzed in ASC and HUVEC or BREC. Total RNA was extracted using Trizol Reagent (Life technologies, Carlsbad, CA) accord-ing to the manufacturer's protocol. Afterward, 1 μg of total RNA was reverse transcribed using the First Strand cDNA syn-thesis kit (Fermentas UAB, Vilnius, Lithuania) according to the manufacturer's instructions. The cDNA equivalent of 5 ng RNA was used for amplification in 384-well microtiter plates in a TaqMAN ABI7900HT cycler (Applied Biosystem, Foster City, CA) in a final reaction volume of 10 μl containing 5 μl SybrGreen universal polymerase chain reaction (PCR) Master Mix (Bio-Rad, Richmond, CA) and 6 mM primer mix (forward and reverse). Cycle threshold (C_T) values for individual reactions were determined using ABI Prism-SDS 2.2 data processing software (Applied Biosystem, Foster City, CA). The C_T values were normalized to GAPDH as a reference gene using the ΔC_T method, normalizing for the expression of the reference gene and related to the control treatment. All cDNA samples were

Table 1. Primer sequence for RT-qPCR

Human	Forward	Reverse
NOTCH1	5′-CGGGGCTAACAAAGATATGC-3′	5′-CACCTTGGCGGTCTCGTA-3′
NOTCH2	5′-TGGTATTGATGCCACCTGAA-3′	5′-GTTGGTGTGGAGCAGGGTA-3′
NOTCH3	5′-CCTGCCATGGAGGGTACA-3′	5′-GCAGGAGCAGGAAAAGGAG-3′
NOTCH4	5′-TCTCCCTGTGCCAATGGT-3′	5′-AGGCACTCATCCACCTCTGT-3′
JAGGED1	5′-TGAGCAAACTTGTGGCCTG-3′	5′-TTACTGCCTCCCATGAACCTG-3′
JAGGED2	5′-GAGGATGAGGAGGACGAGGA-3′	5′-GAGGATGAGGAGGACGAGGA-3′
DLL1	5′-ACTCCGGCTTCAACTGTGAG-3′	5′-ACTCGCACACATAGCGGTG-3′
DLL3	5′-GACCCTCAGCGCTACCTTTT-3′	5′-ACCTCCTCAAGCCCATAGGT-3′
DLL4	5′-GACCACTTCGGCCACTATGT-3′	5′-CCTGTCCACTTTCTTCTCGC-3′
GAPDH	5′-GATCCCTCCAAAATCAAGTG-3′	5′-GCAGAGATGATGACCCTTTT-3′
PDGFR-beta	5′-CCCTTATCATCCTCATCATCG-3′	5′-CCTTCCATCGGATCTCGTAA-3′

Bos Taurus	Forward	Reverse
NOTCH1	5′-CAGCTACGGCACCTACACG-3′	5′-CTGGGCACGTCACAGTAGAG-3′
NOTCH2	5′-CCCACTAGCCTCCCTAACCT-3′	5′-TGCCTTTGGGGATTAGCTGG-3′
NOTCH3	5′-AGAGTGGCGACCTCACCTAT-3′	5′-GCAAACCCCACCGTTAACAC-3′
NOTCH4	5′-GGAGGCTGAAGAAATGGCCT-3′	5′-CAGCTGAGCTACCTCCATCG-3′
JAGGED1	5′-CGGGAAGTGCAAGAGTCAGT-3′	5′-ACAGGGGTTGCTCTCACAGT-3′
JAGGED2	5′-GCTCCTAGAGGCAGATGGTG-3′	5′-GCGGTAGCCATTGATTTCAT-3′
DLL1	5′-GCCAAATGGTCAGTGAGCTG-3′	5′-TCTTGCGGTGAACGTTTTGC-3′
DLL3	5′-GGATGGACCTTGTTTCAACG-3′	5′-CAGTGGCAAATGTAGGCAGA-3′
DLL4	5′-CCTGACAACTTCGTCTGCAA-3′	5′-GCCACCATGCACAGTAACAC-3′
GAPDH	5′-TGACCCCTTCATTGACCTTC-3′	5′-GATCTCGCTCCTGGAAGATG-3′

amplified in duplicate. Primer sequences for quantitative real-time reverse transcriptase–PCR (RT-qPCR) are listed in Table 1.

Lentivirus Transduction

For lentiviral transductions to obtain the *NOTCH2* knockdown, HEK cells were transfected using Endofectin-Lenti (Gene Copoeia, Rockville, MD, EFL-1001-01) with the following plasmids: pLKO.1-SH-NOTCH2 (GE-Healthcare Bio-Science, SE, Sweden) or pLKO.1-SCR, pVSV-G (envelope plasmid) and pCMVΔR8.91 (gag–pol second generation packaging plasmid). A combination of five constructs was tested to improve the chance of downregulation. For *NOTCH2*, two constructs were proven to efficiently knock down NOTCH2 by eightfold at protein level. Virus collection was started the day after transfection. ASC (50% confluent) were transduced in DMEM, 10% FBS, supernatant containing viruses were added for two consecutive days. The first transduction was facilitated with 4 μg/ml polybrene. Transduced cells were allowed to proliferate for another 3 days and were then selected with 2 μg/ml puromycin for at least 7 days. Transduction efficiency for *NOTCH2* (reduced detectable protein by Western blotting analyses) was confirmed for all *NOTCH2* knockdown cultures used in the experiments.

Vessel Network Formation Two Dimensions and Three Dimensions

ASC were plated on 15 mm Termanox coverslips (NUNC, Rochester, NY) at 1×10^4/cm^2 in DMEM, 10% FBS for 24 hours. Next, medium was replaced with ECM for 5 days. HUVEC were seeded on top of ASC monolayers or on gelatin-coated coverslips at 1×10^4/cm^2 in ECM and cultured for 5 days, after which vascular network formation was assessed. Three-dimensional (3D) cocultures were achieved by embedding ASC and HUVEC (3×10^5 cells of each cell population) in 100 μl of Matrigel (Corning, growth factor reduced, New York, NY) accommodated in a 3D printed scaffold (the scaffold was printed with a commercially available 3D printer; Reprap Prusa i3, Anet 3D, China; biodegradable material, polylactic acid, was used to print the scaffolds). Cells were grown for 9 days. HUVEC tubular formation and interconnection were assessed at 24 hours, 27 hours, 6 days, and 9 days. Immunostaining was performed as following. Samples were fixed in 4% paraformaldehyde in PBS for 20 minutes. Subsequently, cells were permeabilized with 1% BSA and 0.5% Triton-X100 in PBS at room temperature for 1 hour at 4°C. After PBS washes, primary antibodies were incubated for 90 minutes: mouse-anti-human-CD31 (1:100, Dako, Glostrup, Denmark), rabbit-anti-human-NOTCH2 (Cell Signaling, Danvers, MA, 4530S). Samples were washed with PBS and incubated with the fluorescein-conjugated-donkey-anti-mouse-IgG (for CD31, PECAM-1) (1:500, Jackson Immunoresearch, U.K.) and to fluorescein-conjugated-goat-anti-rabbit IgG (for NOTCH2) (1:500, Jackson Immunoresearch, U.K.) in PBS containing 4′,6-diamidino-2-phenylindole (DAPI). For colocalization staining in both two dimensions (2D) and 3D, ASC were CM-DiI-labeled (Thermo Fisher Scientific, Vybrant CM-DiI red Molecular Probes, Sanbio, Uden, The Netherlands), whereas HUVEC were staining for CD31. 2D VNF images were acquired by automated microscope TissueFAXS. Confocal microscope (SP8) was used to acquire *z*-stack images at ×63. Post-processing for imaging was achieved using ImageJ free software [28]. 3D scaffolds were designed with SketchUp 2016 software. 3D VNF were reconstructed by imageJ 3D viewer plugin.

Immunoblotting

Cells were lysed in radioimmunoprecipitation assay buffer (RIPA buffer) (Thermo Fisher Scientific, Waltham, MA), freshly supplemented with proteinase inhibitor cocktail and phosphatase inhibitor cocktails-2 and 3 (all from Sigma-Aldrich, St. Louis, MO). A total of 10 μg of protein per sample was loaded in each lane. Electrophoresis was performed in 10% polyacrylamide gels, followed by electrotransfer onto nitrocellulose membranes (Corning with semidry Transblot Turbo system (Bio-Rad). Membranes were blocked with Odyssey Blocking

Buffer (Li-COR Biosciences, Lincoln, NE) diluted 1:1 in Tris-buffered Saline (TBS) at room temperature for 1 hour.

Blots were then incubated with primary antibodies at 4°C, overnight, and after washing with TBS, with secondary antibodies at room temperature for 1 hour. The membranes were washed three times with TBS with 0.1% Tween in between incubations and additionally with TBS before the scanning. Visualization of bound secondary antibodies was done with an Odyssey scanner (Li-COR Biosciences, Lincoln, NE) and digital images were captured. These were analyzed with Odyssey software (Li-COR Biosciences, Lincoln, NE), and densitometry was performed with TotalLab 120 software (Nonlinear Dynamics, Newcastle, U.K.). Images depicted in figures were processed in Adobe Photoshop and Illustrator, and if necessary, brightness of a whole image was adjusted in linear fashion for display purposes only (Adobe Systems Incorporated, San Jose, CA).

The following antibodies were used: Rabbit NOTCH2 (1:1,000, Cell Signaling, Danvers, MA, 4530S), Rabbit platelet-derived growth factor receptor beta (PDGFRB) (1:250, Santa Cruz Biotechnology, Dallas, TX, sc-432), Mouse monoclonal GAPDH (1:1,000, Abcam, Cambridge, U.K., ab9485 or ab9484), anti-rabbit IgG IRDye-680LT (1:10,000, Li-COR Biosciences, Lincoln, NE, 92668021).

Migration Assay

Migration toward chemoattractant PDGF-BB (Recombinant human PDGF-BB, Peprotech, Inc., NJ), as well as to conditioned media of HUVEC and BREC was measured using a 48-well micro chemotaxis chamber with 8 μm pore size filters (Neuro probe, MD). A concentration of 20 ng/ml PDGF-BB proved optimal for migration and was used in further experiments. HUVEC and BREC were cultured in RPMI. Twenty-four hours later, medium was collected and filtered with a 20 μm filter (Corning, New York). The lower chamber contained RPMI supplemented with PDGF-BB, HUVEC and BREC conditioned medium, 8×10^3 cultured ASC, ASC SH-SCR [Scramble] and ASC SH-NOTCH2 were placed in the upper chamber. After incubation at 37°C for 4 hours, migrated cells were fixed and stained with DAPI (Sigma, MO). Nuclei were counted in representative high power fields (12 chemotaxis chambers were quantified per condition, $n = 3$ independent experiments) visualized with ×40 objective magnification per sample.

Adhesion Assays

Single cell suspensions of ASC were seeded on confluent monolayers of HUVEC and monitored respectively for 8 hours (adhesion) and 36 hours (adhesion and proliferation). CM-DiI labeled ASC (Thermo Fisher Scientific, Vybrant CM-DiI Molecular Probes, Sanbio, Uden, The Netherlands) were used to discriminate ASC from HUVEC. At the end of the incubation, the cocultures were gently washed and fixed with 4% paraformaldehyde in PBS for 20 minutes. Nuclei were stained with DAPI. Stained nuclei and adhered red-labeled ASC were counted using an automated microscope TissueFAXS (TissueGnostics, Vienna, Austria).

Proliferation Assay

ASC (WT, SH-SCR, and SH-NOTCH2) were cultured in RPMI medium until confluency. Twenty-four hours after replacing fresh RPMI, medium was collected and filtered with a 20 μm

filter (Corning, New York). HUVEC were seeded at 1×10^4 cells/cm^2 and allowed to attach for 2 hours before conditioned medium was added. After 3 days with ASC conditioned medium treatment, HUVEC were stained with a marker for proliferative cells (Anti-Ki67 antibody ab15580, 1:250, Abcam). Four field of views from four replicates per condition were quantified. ImageJ software was used to split colors. The images displaying Ki67 staining were transformed to 8-bit. To each image a threshold was applied. The pixels' area of Ki67 positive nuclei was quantified ($n = 3$ independent experiments).

Animals and Oxygen-Induced Retinopathy Model

All animal experiments in this study were approved by the Institutional Animal Care and Use Committee (Regierungspräsidium Karlsruhe, Germany) and were performed according to guidelines of the statement of animal experimentation issued by the Association for Research in Vision and Ophthalmology (ARVO). C57Bl/6J mice were housed in groups in cages with free access to standard chow and water under 12 hours light and 12 hours dark rhythm. To study the influence of ASC on hyperoxic vasoregression and subsequent hypoxia-driven angiogenesis, newborn mice, female, and male were used to assess the migration and engraftment of ASC that were administered intravitreally. Mice at postnatal day 7 were exposed to 75% oxygen atmosphere for 5 days with their nursing mother, and then returned to room air (an ~20% oxygen) at postnatal day 12. Directly after return to room air, randomly selected mice were intravitreally injected with either 0.5 μl of PBS containing 7×10^3 ASC (WT, SH-SCR, and SH-NOTCH2) or 0.5 μl PBS alone as control (Hamilton, Microliter Syringes). At P19, mice were under deep anesthesia for ERG analysis and for quantification of neovascularization, subsequently mice eyes were enucleated. After collection, eyes were either fixed in 4% buffered formalin or snap frozen and stored at 80°C for later analysis. Whole mount retinas from P19 animals were permeabilized by treatment with 1% BSA and 0.5% Triton-X100 in PBS at room temperature for 1 hour. Overnight staining was with FITC- or TRITC-labeled isolectin-B4 (Sigma, 1:50) at 4°C. After PBS washes, retinas were flatmounted in 50% glycerol and subsequently stained for microvasculature with Lectin-FITC (1/70, Sigma-Aldrich, Saint Louis, MO). Retinal capillaries and CM-DiI-labeled ASC (red) were acquired with a fluorescence microscope (Leica BMR, Bensheim, Germany). Alternatively, confocal laser scanning microscopy was used (Leica TCS SP2 Confocal Microscope, Leica, Wetzlar, Germany) to assess (co-)localization of Lectin-TRITC-stained microvasculature and CM-DiI-labeled ASC.

Multifocal Electroretinogram

Multifocal electroretinography was performed as previously described [29]. The mice were placed in front of the scanning laser ophthalmoscope device (RETImap, Roland Consult, Brandenburg, Germany), with a drift tube linac (DTL) electrode placed at the cornea. Subcutaneous silver needle electrodes were positioned at the neck of the mice serving as reference and ground electrodes. A 90 dpt (dioptrie) contact lens (Volk Optical, Inc., Mentor, OH) mounted over viscous 2% Methocel gel (OmniVision GmbH, Puchheim, Germany) was placed on the eyes of the mice. An array of 19 equally sized hexagons
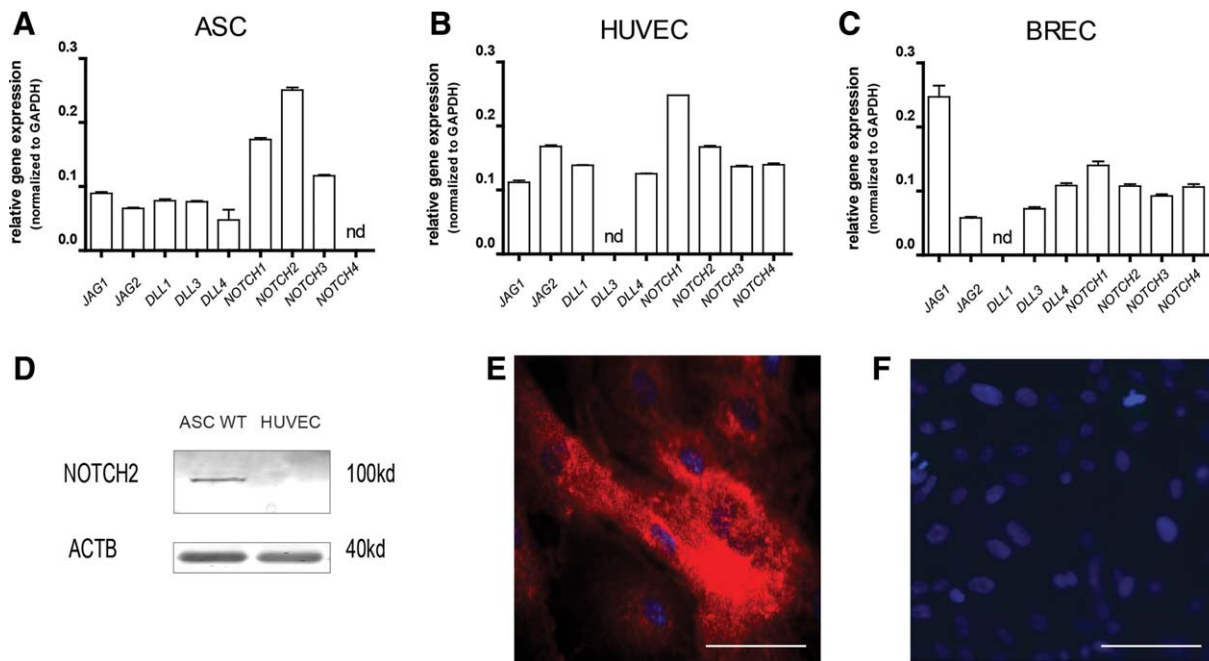
Figure 1. ASC predominantly express NOTCH2. Confluent monolayer of ASC cultured in hyperglycemic conditions were harvested and messenger RNA isolated. Relative gene expression of Notch members was determined using RT-qPCR in **(A)** ASC, **(B)** HUVEC, and **(C)** BREC. Gene expression was normalized to the reference gene GAPDH ($n = 4$). **(D):** NOTCH2 was detected at protein level by Western blot in ASC WT and HUVEC. NOTCH2 was detected as a 100 kDa band. Immunofluorescence detection of NOTCH2 protein on **(E)** cultured ASC and **(F)** HUVEC. Images are representative for $n = 3$ replicates. Scale bars: 50 μm. Abbreviations: ASC, adipose tissue-derived stromal cells; BREC, Bovine retinal endothelial cells; HUVEC, human umbilical cord vein endothelial cells; nd, not detectable; RT-qPCR, real-time polymerase chain reaction.

was chosen and stimulation was performed using 150 cd/m^2 and 1 cd/m^2 for the m-sequence with four dark frames in between the stimuli. An average of eight cycles was used for the final analyses. Multifocal electroretinogram (mfERG) recording took place under photopic conditions where, in mice, both rod and cone photoreceptors were activated. The initial negative-going a-wave is initiated by photoreceptors, whereas the following positive-going b-wave is generated in the inner retina, mainly by ON-bipolar cells.

Statistical Analysis

All the data are presented as a mean with SD and were analyzed using GraphPad Prism 5 (GraphPad Software, Inc.). Statistical significance was determined using either one-way analysis of variance (ANOVA) with Bonferroni post hoc or Student's t test analysis depending on the experimental conditions. Values of $p < .05$ were considered statistically significant.

RESULTS

Assessment of Notch Components Expression by ASC

The Notch family comprises five ligands and four receptors in mammals. We characterized their basal gene expression in ASC (Fig. 1A), BREC and HUVEC (Fig. 1B, 1C). The expression of *JAG1, JAG2, DLL1, DLL3,* and *DLL4* was detected in C_T values not greater than 0.1 in ASC. In contrast, gene expression of the Notch receptors varied in ASC. *NOTCH2* had the highest expression (C_T value 0.251 ± 0.09 normalized to *GAPDH*), followed by *NOTCH1* (0.173 ± 0.006), and *NOTCH3* (0.117 ± 0.003) while *NOTCH4* had either very low expression levels or was not

detectable depending on the ASC donor pool that was assessed.

The expression levels of *JAG1, JAG2, DLL1, DLL4* ligands and *NOTCH2, NOTCH3,* and *NOTCH4* receptors were all similar in HUVEC when compared with one another. Expression of *DLL3* was not detectable, while *NOTCH1* had the highest expression (0.248 ± 0.033). In contrast, in BREC, expression of *JAG1* was highest (0.247 ± 0.043) compared to *JAG2* (0.068 ± 0.004). *DLL1* expression was not detectable, while expression of *DLL3* and *DLL4* was similar to *JAG2*. *NOTCH2* expression by ASC was confirmed at the protein level (Fig. 1D). Besides, NOTCH2 protein was not expressed in HUVEC (Fig. 1D). Immunohistochemistry on ASC and HUVEC confirmed NOTCH2 in ASC and NOTCH2 absence in HUVEC, respectively (Fig. 1E, 1F).

The maintenance of ASC in normoglycemic (5 mM glucose) or hyperglycemic medium (25 mM glucose) from isolation onward, did not influence the expression of *JAG1*, nor *NOTCH1–4* (Supporting Information Fig. S1), while expression of *NOTCH2* was again higher than expression of the other members. Therefore, our investigations focused on *NOTCH2*.

NOTCH2 Downregulation Inhibits ASC's Capacity to Sustain Vessel Network Formation in 2D and 3D

The role of Notch signaling in controlling the sprouting of nascent vessels during angiogenesis is well characterized [30]. The pattern of Notch receptors and ligands expression on EC and pericytes is a regulated mechanism that controls new vessel development and homeostasis. NOTCH2 receptor expression on ASC may represent a possible mediator of ASC pericytic features. In order to test this hypothesis, we
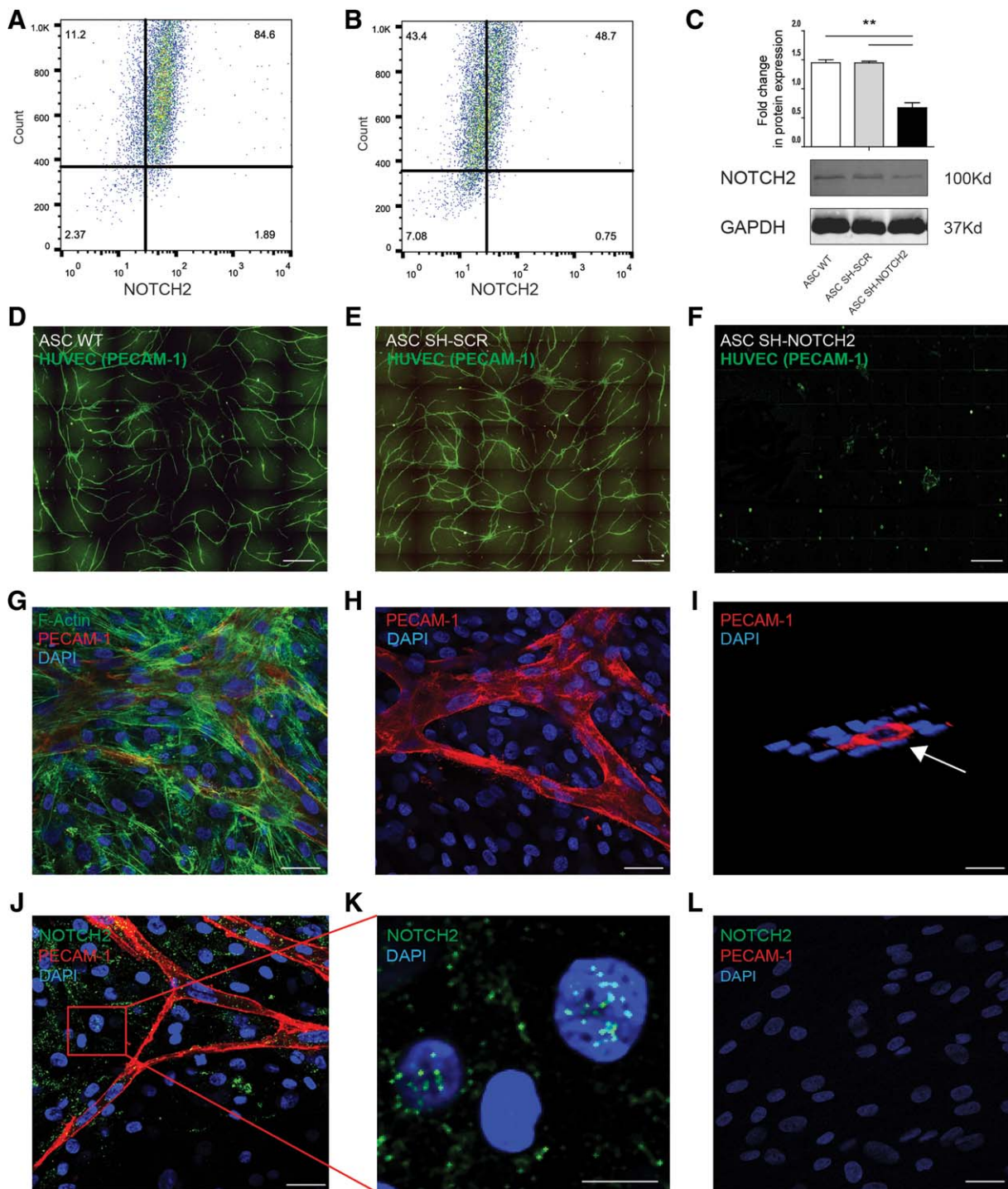
Figure 2. SH-NOTCH2 ASC suppresses endothelial cells network formation in 2D. ASC were lentiviral transduced with SH-NOTCH2 vector and SH-SCR control vector. ASC were stained for NOTCH2 and flow cytometry was used to measure the changes in surface expression. Representative FACS plots showing percentage of positive cells, in ASC WT **(A)** and in ASC SH-NOTCH2 **(B)**. The data are representative of two independent experiments analyzed with FlowJo V10 software (1×10^4 cells analyzed per experimental condition). **(C):** VNF of HUVEC (PECAM-1, green) cultured for fourteen days on **(D)** ASC WT, **(E)** ASC SHSCR, and **(F)** ASC SH-NOTCH2. **(G):** HUVEC grown on ASC WT monolayer stained for actin filaments (phalloidin-FITC, green) and membrane protein PECAM-1 (red). **(H):** Image processing for removal of F-actin, using imageJ software. HUVEC interconnected network laying between ASC were extracted from a *z*-stack acquisition. **(I):** Lumen formed by HUVEC cultured on ASC-WT. **(J):** Detection of NOTCH2 expression in ASC WT-driven HUVEC (PECAM-1) VNF. Inset **(K)** high magnification of NOTCH2 expression in ASC WT supported HUVEC VNF. **(L):** Detection of NOTCH2 expression in ASC SH-NOTCH2 supported HUVEC VNF. The panels (D, E) were composed by stitching together 25 high magnification ($\times$40) micrographs obtained by automated microscopy (TissueFAXS). Each experimental condition had three different ASC donors pooled together. The images are representative for three independent experiments. Scale bar (D–F) 1 mm, (G–J, L) 20 μm, (K) 10 μm. **, $p \leq .01$, *t* test. Abbreviations: ASC, adipose tissue-derived stromal cells; DAPI, 4′,6-diamidino-2-phenylindole; FACS, fluorescence-activated cell sorter; FITC, fluorescein isothiocyanate; HUVEC, human umbilical cord vein endothelial cells; VNF, vascular(-like) network formation.
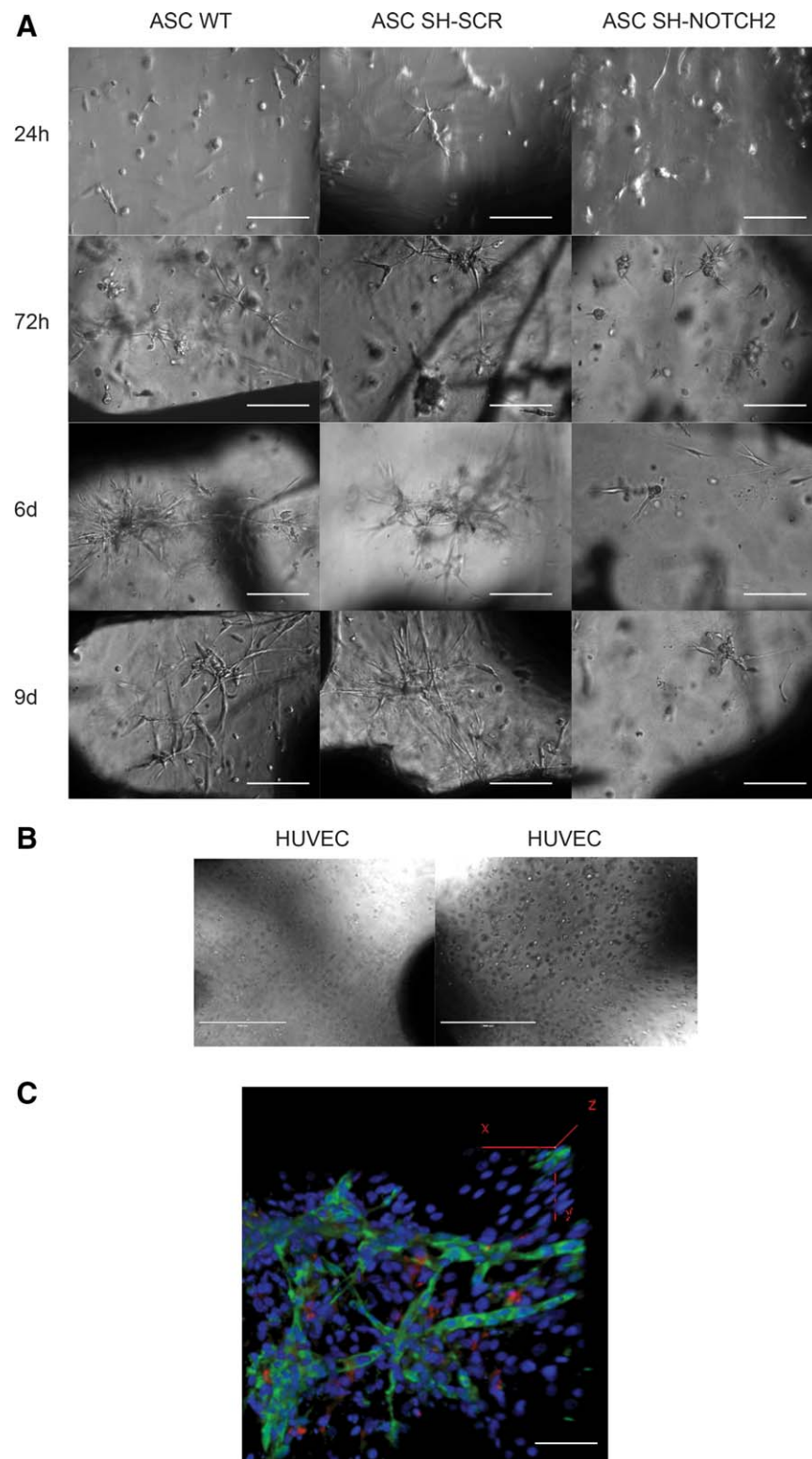
Figure 3. ASC SH-NOTCH2 dynamics in 3D microenvironments. ASC and HUVEC (1 to 2 ratio) at a total density of 3 $\times$ 10^5 cells were embedded in Matrigel. **(A):** ASC WT, ASC SH-SCR, and ASC-SH-NOTCH2 were cocultures with HUVEC and monitored for respectively 1, 3, 6, and 9 days. A bright field microscope was used to acquire images. Field of view $\times$20 magnification. **(B):** HUVEC seeded alone at a total density of 2 $\times$ 10^5 cells (low) and 3 $\times$ 10^5 cells (high density) were embedded in Matrigel and cultured for 5 days. HUVEC remained round-shaped and no protrusions indicate of network formation were observed. **(C):** Three-dimensional reconstruction of vessel-like network formation of ASC (CM-DiI-labeled, red) and HUVEC (PECAM-1, green). Nuclei were stained with 4′,6-diamidino-2-phe-nylindole (blue). Confocal microscopy with z-stack acquisition was used to reconstruct the image. Scale bar: (A) 100 μm, (B) 400 μm, and (C) 50 μm. Abbreviations: ASC, adipose tissue-derived stromal cells; HUVEC, human umbilical cord vein endothelial cells.

investigated the capacity of ASC to support HUVEC vessel formation in 2D and 3D.

A short hairpin against NOTCH2 was lentiviral transduced in ASC to reduce its expression. The 85% of control ASC showed surface expression of NOTCH2 (Fig. 2A), while in ASC-SH-NOTCH2, 44% of cells had no detectable surface expression and the remainder had a significantly reduced surface expression of NOTCH2 (Fig. 2B). NOTCH2 downregulation in ASC SH-NOTCH2 is further confirmed at protein level (Fig. 2C).

Confluent monolayers of ASC wild type (ASC WT) and ASC transduced with a scrambled control (ASC SH-SCR) supported vascular network formation (VNF) by HUVEC (Fig. 2D, 2E),

corroborating our previous data [31]. Thus, the lentiviral transduction by itself did not affect VNF. HUVEC formed an interconnected branched network on the ASC monolayer which remained stable for at least 14 days. In contrast, monolayers of ASC reduced NOTCH2 surface expression (SH-NOTCH2) did not support VNF by HUVEC (Fig. 2F). HUVEC that had precipitated by gravity on the ASC SH-NOTCH2 monolayer at best formed small clusters rather than tubular networks. However, lack of contact caused death of most seeded HUVEC (not shown). Confocal laser scanning microscopy revealed that the ASC adhered to and wrapped around the tubular structures formed by the HUVEC (Fig. 2G). By focusing on the focal plane in which the HUVEC were located (Fig. 2H), the defined tubular structure of the HUVEC identified through positive staining for PECAM-1 (red) could be seen surrounded by the ASC. By using reconstructed Z-stacks from transversal optical sections, the tubes were confirmed to harbor a lumen (Fig. 2I). ASC in the vicinity of the HUVEC tubular structures, had intranuclear expression of NOTCH2, indicating that NOTCH2 was activated in these cells (Fig. 2J). Nuclear translocation and localization of NOTCH2 is showed in Figure 2K. NOTCH2 was not detected in ASC SH-NOTCH2 monolayers (Fig. 2L).

VNF is a valuable tool to assess vasculogenesis in vitro. However, this assay is limited in its nature as it is not truly reflective of the 3D environment cells experience in vivo. To address this limitation the influence of ASC on vasculogenesis, this process was investigated in a 3D printed scaffold microenvironment. The scaffold was used as a biodegradable container which allowed the Matrigel to be held in place. ASC WT, SH-SCR, or SH-NOTCH2 were seeded and cocultured with HUVEC in Matrigel supported by a 3D printed poly-lactic acid scaffold and followed for nine days (Fig. 3). Within this time, ASC WT and ASC-SH SCR supported HUVEC to form an interconnected branching network. In contrast and similar to their performance in 2D, ASC SH-NOTCH2 did not support the formation of networks by co-seeded HUVEC (Fig. 3A). Importantly, HUVEC alone did not sprout or form networks when embedded in Matrigel at either a lower or high seeding density (Fig. 3B, right panel lower density and left panel higher density, respectively), confirming the important role of ASC in inducing the vasculogenic process. 3D image reconstruction of the VNF showed the CD31 (PECAM-1) positive HUVEC (green)
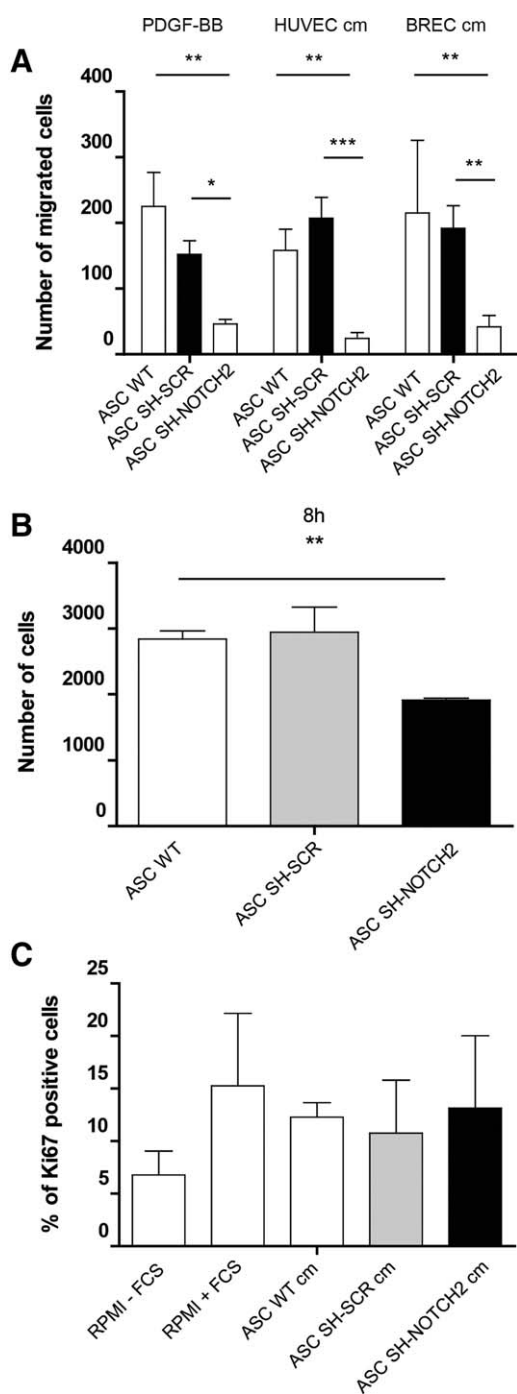
Figure 4. NOTCH2 is required for migration of ASC and their adhesion to endothelial cells, whereas endothelial cell proliferation is not affected. Medium containing PDGF-BB, HUVEC secretome, and BREC secretome was collected. ASC were cultured with standard medium and a neuroprobe system was used to measure ASC migration toward conditioned medium **(A)** ASC (WT, SH-SCR, and SH-NOTCH2) migration toward PDGF-BB as well as conditioned medium derived from BREC and HUVEC **(B)** Adhesion of ASC (WT, SH-SCR, and SHNOTCH2) on endothelial cells monolayer after 8 hours. **(C):** ASC (WT, SH-SCR, and SH-NOTCH2) conditioned medium was collected. Proliferation of endothelial cells treated with ASC conditioned medium was detected by Ki67 staining. ImageJ software was used to split colors. The images displaying Ki67 staining were transformed to 8-bit. To each image, a threshold was applied. The pixels' area of Ki67 positive nucleus were quantified ($n = 3$ independent experiments). *, $p \leq .05$, **, $p \leq .01$, ***, $p \leq .001$, unpaired t test and one-way ANOVA. Abbreviations: ANOVA, analysis of variance; ASC, adipose tissue-derived stromal cells; BREC, Bovine retinal endothelial cells; HUVEC, human umbilical cord vein endothelial cells.

generated tubular structures supported by the ASC (red CM-DiI label, Fig. 3C).

PDGFRB, Migration and Adhesion Are Reduced in ASC SH-NOTCH2

To further examine the role of NOTCH2 in the ASC pericytic-like phenotype, their migratory capacity was investigated. Conditioned media from cultured HUVEC and BREC were used as chemoattractant. In addition, PDGF-BB, known to be an EC-secreted chemoattractant for pericytes, was used as a positive control. Wild type ASC and ASC SH-SCR migrated toward PDGF-BB in a similar fashion and also migrated similarly toward conditioned media of HUVEC or BREC (Fig. 4A). In contrast, the migration of ASC SH-NOTCH2 was four- to five-fold lower toward PDGF-BB or conditioned media of HUVEC or BREC, compared to either control media ($p \leq .01$, $p \leq .001$, Fig. 4A). In addition to the reduced responsiveness to chemo-attractant of ASC SH-NOTCH2, their adhesion to HUVEC was also reduced (Fig. 4B). The adhesion of ASC SH-NOTCH2 was approximately 30% lower than ASC WT and ASC SH-SCR ($p \leq .5$; $p \leq .01$, Fig. 4B). Yet, knockdown of *NOTCH2* did not influence other paracrine signaling by ASC: the proliferation (Ki67) of HUVEC was similar in conditioned media from control ASC and ASC SH-NOTCH2 (Fig. 4C).

Because ASC SH-NOTCH2 had reduced migration toward EC-secreted chemoattractants and PDGF-BB, the expression of the receptor for PDGF (PDGFRB) was determined in ASC. Expression of *PDGFRB* was reduced sixfold ($p \leq .001$, Fig. 5A) in ASC SH-NOTCH2 compared to ASC WT. At the protein level, expression of PDGFRB by ASC SH-NOTCH2 was also reduced when compared to ASC WT or ASC SH-SCR controls ($p \leq .5$, Fig. 5B, protein quantification Fig. 5C).

ASC SH-NOTCH2 Do Not Acquire Pericytic Position in the Oxygen-Induced Retinopathy Retinal Microvasculature, but Maintain Paracrine Pro-Regenerative Capacity

In order to verify the findings obtained in vitro, ASC (WT, SH-SCR, and SH-NOTCH2) were injected in eyes of mice with oxygen-induced retinopathy (OIR). In this mouse model, pups are exposed to hyperoxia while the retinal vasculature is still developing. The subsequent return of pups at room air (an ~20% oxygen) prompts excessive pathological angiogenesis [32]. Control ASC (WT and SH-SCR) and ASC SH-NOTCH2 were injected intravitreally at P7 immediately after 5 days of hyperoxia. Avascular areas in whole mount retinas were quantified at P19. Animals which had not received any ASC injection had large avascular areas in the central retina (Fig. 6A). The administration of ASC WT, the scrambled control (ASC-SCR), and SHNOTCH2 largely restored the avascular areas (untreated animals avascular areas: 50,000 μm^2; ASC treated animals avascular areas: 10,000 μm^2). It appeared that the lentiviral integration by itself reduced the capacity to fully revascularize the central retina, because a complete central retinal micro-vasculature reconstitution was not observed (Fig. 6B–6D). To further assess the functional status of retinal cell layers after ASC-induced revascularization, mfERG was performed and a-waves (photoreceptor function) and b-waves (inner retinal function) were measured in avascular, vascular, and neovascular areas. With regard to avascular areas, a-waves measured in ASC WT, ASC SH-SCR, and ASC SH-NOTCH2 showed an
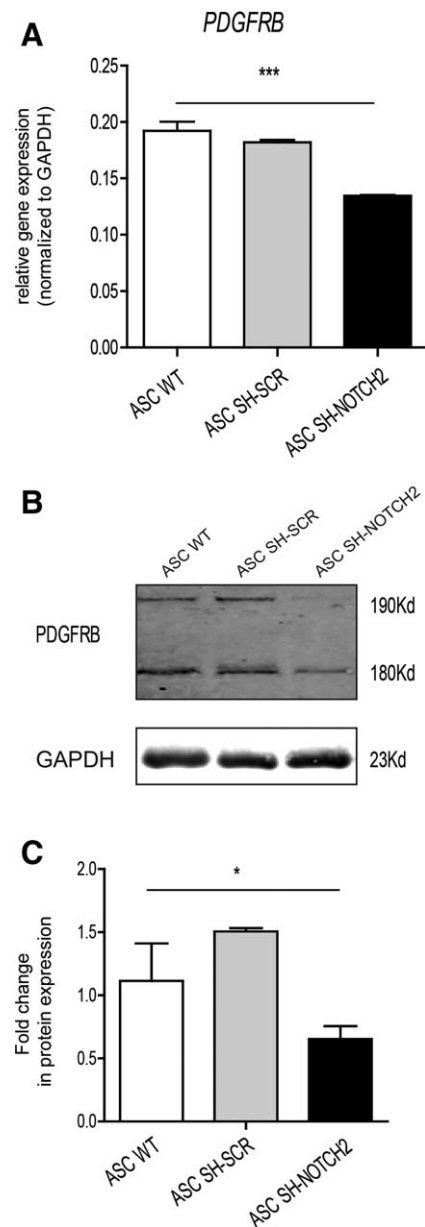

Figure 5. NOTCH2 knockdown reduces PDGFRB expression on ASC. Confluent monolayer of ASC (WT, SH-SCR, and SH-NOTCH2) were lysed with trizol for mRNA isolation and RIPA buffer for protein isolation. RT-qPCR was performed and immunoblotting were performed, respectively. **(A):** Gene expression of PDGFRB. Expression of GAPDH was used as reference gene for normalization. **(B):** Immunoblotting of PDGFRB expression detected as two bands of respectively 190 kDa and 180 kDa. **(C):** PDGFRB protein expression quantification in ASC (WT, SH-SCR, and SH-NOTCH2). The bands obtained were normalized to GAPDH and quantified by ImageJ gel analyzer. *, $p \leq .05$, ***, $p \leq .001$, t test. Abbreviations: ASC, adipose tissue-derived stromal cells; PDGFRB, platelet-derived growth factor receptor beta; RIPA, radioimmunoprecipitation assay; RT-qPCR, Real-Time Polymerase chain reaction.

increase in amplitude when compared to untreated eyes ($p \leq .01$, Supporting Information Fig. S2A). Subsequently, b-wave amplitudes measured in the avascular areas showed significant increment when ASC WT were injected in the eyes and compared to ASC untreated animals ($p \leq .5$, Supporting Information Fig. S2B). In contrast, ASC SH-SCR and ASC SH-
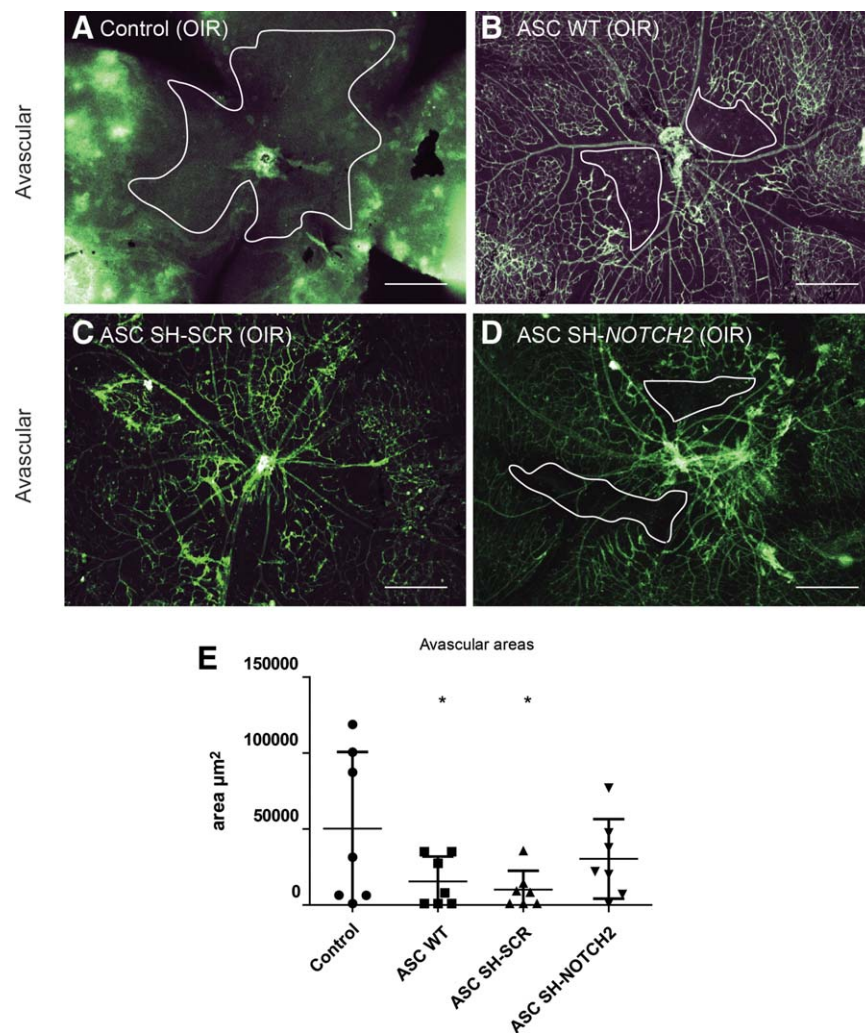
Figure 6. ASC SH-NOTCH2 partially recovered avascular area in the retina. Five days old C57BL/6 mice were exposed to 75% of oxygen for 5 days and then returned to room air (an ∼20% oxygen). ASC (WT, SH-SCR, and SH-NOTCH2) (7 × 10³ cells/0.5 µl) were injected at day 7. Retina whole mounts were prepared on day 19. Representative whole mount retinas derived from **(A)** untreated mouse, **(B)** animals with injection of WT ASC, **(C)** mice with injection of ASC SH-SCR, **(D)** mice with injection of ASC SH-NOTCH2. Avascular area is marked by a white closed line. **(E):** Avascular area quantification, $n = 7$ animals per group. Significant difference between ASC WT and ASC SH-SCR compared with untreated animals and ASC SH-NOTCH2. *, $p \leq .05$, t test. Scale bars: 500 µm. Images are representative of results seen in $n = 7$ animals in each group. Abbreviations: ASC, adipose tissue-derived stromal cells; OIR, oxygen-induced retinopathy.

NOTCH2 showed no difference among the groups. There were no differences detected in the a-wave and b-wave amplitudes measured in the vascular and neovacular zones across the groups (Supporting Information Fig. S2C–S2F).

Imaging analyses performed on P19 mice retinas showed that control ASC (Supporting Information Fig. S3, red) were homogeneously distributed around the microvasculature (green) in the retina. Control ASC (WT) had adhered to typical pericytic positions on the retinal capillaries, that is, on branching points and around capillaries (arrow heads, Supporting Information Fig. S3). Similarly, ASC SH-SCR controls also adhered at pericytic positions. In contrast, intravitreally administered ASC SH-NOTCH2 did not reach the retinal microvasculature, but formed intravitreal aggregates (Supporting Information Fig. S3).

DISCUSSION

This study demonstrates that Notch signaling is fundamental for ASC pericytic interaction and therapeutic function in the context of pathological retinal vasoproliferation. Specifically, NOTCH2 is essential for in vitro vascularization and subsequent stabilization. In addition, the expression of the Notch receptors and JAGGED1 ligand were refractory to HG. Both in vitro and in vivo, NOTCH2 promotes expression of PDGFRB on ASC which proved crucial for the EC-driven chemoattraction of ASC. Finally, NOTCH2 does not affect the pro-angiogenic paracrine function of ASC because in vivo, both ASC WT and ASC SH-NOTCH2 showed reconstitution of capillary beds. However, ASC with reduced NOTCH2 expression appeared to have lost their migratory capacities when introduced in an ischemic and neo-vascularized retinal microenvironment.

To date, few studies have investigated the molecular mechanisms that orchestrate ASC and their interaction with the retinal microvasculature [33, 34]. In contrast, the role of Notch signaling in angiogenesis is well-established [30]. Benedito et al. [35] concluded that Notch signaling modulates VEGFR2 and VEGFR3 in different manners in retinal EC. A specific Notch receptor was not identified in this study, however,

the overall Notch activity was ablated by gamma secretase inhibitor. They reported that *VEGFR3* activation depends on both the Notch and *VEGFR2-VEGF* axis to promote angiogenesis on nascent vessels. Notch signaling alone was not sufficient to induce *VEGFR2* activation. The latter suggests that more upstream regulators might be involved in cell-to-matrix interaction. In the current study, we show that genetic disruption of *NOTCH2* in ASC prevents "docking" of EC to ASC and vice versa in vitro. Interestingly, in a 3D coculture system, NOTCH2 proved essential to promote vasculogenic behavior of HUVEC. The knockdown of *NOTCH2* completely abrogated network formation by HUVEC.

It is well-known that endothelial-secreted PDGF-BB serves as a request for mural cell support during vasculogenesis and angiogenesis [36]. Our results show that NOTCH2 regulates the expression of PDGFRB on ASC, which is a prime chemotactic receptor of mural cells, that is, pericytes [37]. The retina has a specialized form of the blood brain barrier and the inhibition of PDGFRB signaling in developing murine retinas disrupted transendothelial barriers and caused vascular leakage [38], very similar to blood-retina barrier (BRB) changes in DR. This is likely due to the lack of sufficient support by pericytes. Our experiments demonstrate the importance of NOTCH2 expression in the regulation of PDGFRB and as a consequence in the regulation of vasculogenesis and angiogenesis. The migration of ASC toward PDGF-BB but also to secreted factors from HUVEC and more importantly from retinal EC (BREC) depended on NOTCH2 signaling. Similarly, the ASC engraft required NOTCH2 expression and signaling. In fact, we observed ASC expressing NOTCH2 in the nucleus in the vicinity of the vasculature. The juxtacrine interaction between ASC and EC depended on NOTCH2 signaling, yet the paracrine influence of ASC on EC was not. On one hand, we showed that the proliferation of EC in vitro was not affected by conditioned medium of ASC SH-NOTCH2. On the other hand, in vivo, the restoration of avascular areas in OIR retinas, was virtually similar between controls and ASC SH-NOTCH2-injected animal eyes. However, the latter did not engraft in the retinal vasculature. The engraftment of ASC WT and accompanied vascular restoration corroborates findings of others [39].

Initial a-waves, which are predominantly rod driven in rodents, were higher in amplitude in avascular areas when both ASC WT and ASC SH-NOTCH2 were injected compared with untreated animals. In contrast, there were no differences in the a-wave amplitude in neovascular and vascular areas. These data are in agreement with findings of others [40, 41], which showed that human bone marrow MSC preferentially migrate toward sites of injury in the retina. The choice of the OIR mouse model was important from the perspective of cell engraftment. In this model the retinal vasculature is still in development [32], conferring a more accessible microenvironment for exogenous cells' homing. Notably, the ischemia-induced retinal neovascularization in this model is not caused by HG. However, retinal ischemia, pre-retinal neovascularization and retinal gliosis, are all reproducible characteristic of DR applicable to the OIR mouse model [42]. In fact, we demonstrated that ASC SH-NOTCH2, retained the therapeutic capacities without physically interacting with inner layers of the retina microvasculature. Whether the latter finding is driven by PDGFRB downregulation or another mechanism is currently unknown. Moreover, positive b-wave generated by

ON-bipolar cells showed significantly improved amplitude upon ASC injection. Specifically, avascular areas measured upon ASC WT or ASC SH-NOTCH2 injection, displayed the same order of improvement in b-wave compared with untreated animals. This finding indicates that ASC SH-NOTCH2 secretome influenced the retinal microenvironment. This event might be attributed to either a direct downregulation of NOTCH2 in ASC, or a combinatorial effect of NOTCH2 downregulation and the impaired retinal microenvironment apply on ASC. Being more in favor of the latter, these observations suggest a role for both paracrine and juxtacrine signaling for the proper functioning of ASC in the retinal microenvironment. A summary of the process investigated in this study showed the importance of retinal chemoattractant to recruit ASC. Alternatively, ASC juxtacrine signals are equally fundamental as the paracrine signals in order to adapt to the retinal microenvironment.

CONCLUSION

Our results demonstrate the intrinsic capacity of ASC to promote, orchestrate, and sustain endothelial cell networks through an evolutionary conserved mechanism, namely Notch signaling. Moreover, the 3D coculture assay showed temporal dynamics of ASC driven vasculogenesis in vitro. Importantly, Notch components on ASC are not affected by HG. The latter combined with in vivo experiments, suggested that ASC are promising for therapeutic intervention in DR but more research is needed to understand the ASC response to signals from the pathological extracellular microenvironment into the diabetic retina. Finally, we propose that molecular intervention is fundamental to improve and understand the ASC regenerative armamentarium.

AUTHOR CONTRIBUTIONS

V.T.: concept and design, collection, data analysis and interpretation, manuscript writing, final approval of manuscript; M.K.: animal experiments analysis and interpretation, final approval of manuscript; J.K.B.: data interpretation and manuscript writing, final approval of manuscript; H.-P.H.: concept of study, financial support, revision of manuscript, final approval of manuscript; M.C.H.: concept and design, manuscript writing, financial support, final approval of manuscript.

DISCLOSURE OF POTENTIAL CONFLICTS OF INTEREST

The authors indicated no potential conflicts of interest.

REFERENCES

1 Duh EJ, Sun JK, Stitt AW. Diabetic retinopathy: Current understanding, mechanisms, and treatment strategies. JCI Insight 2017;2:e93751.

2 Pfister F, Feng Y, Vom Hagen F et al. Pericyte migration: A novel mechanism of pericyte loss in experimental diabetic retinopathy. Diabetes 2008;57:2495–2502.

3 Owens GK, Kumar MS, Wamhoff BR. Molecular regulation of vascular smooth muscle cell differentiation in development and disease. Physiol Rev 2004;84:767–801.

4 Trost A, Lange S, Schroedl F et al. Brain and retinal pericytes: Origin, function and role. Front Cell Neurosci 2016;10:20.

5 Bourin P, Bunnell BA, Casteilla L et al. Stromal cells from the adipose tissue-derived stromal vascular fraction and culture expanded adipose tissue-derived stromal/stem cells: A joint statement of the International Federation for Adipose Therapeutics and Science (IFATS) and the International Society for Cellular Therapy (ISCT). Cytotherapy 2013;15:641–648.

6 Peng L, Jia Z, Yin X et al. Comparative analysis of mesenchymal stem cells from bone marrow, cartilage, and adipose tissue. Stem Cells Dev 2008;17:761–773.

7 Busser H, Najar M, Raicevic G et al. Isolation and characterization of human mesenchymal stromal cell subpopulations: Comparison of bone marrow and adipose tissue. Stem Cells Dev 2015;24:2142–2157.

8 Parvizi M, Plantinga JA, van Speuwel-Goossens CA et al. Development of recombinant collagen-peptide-based vehicles for delivery of adipose-derived stromal cells. J Biomed Mater Res A 2016;104:503–516.

9 Bravo B, Garcia de Durango C, Gonzalez A et al. Opposite effects of mechanical action of fluid flow on proangiogenic factor secretion from human adipose-derived stem cells with and without oxidative stress. J Cell Physiol 2017;232:2158–2167.

10 Oses C, Olivares B, Ezquer M et al. Preconditioning of adipose tissue-derived mesenchymal stem cells with deferoxamine increases the production of pro-angiogenic, neuroprotective and anti-inflammatory factors: Potential application in the treatment of diabetic neuropathy. PLoS One 2017;12:e0178011.

11 Boxall SA Jones E. Markers for characterization of bone marrow multipotential stromal cells. Stem Cells Int 2012;2012:975871.

12 Glenn JD, Whartenby KA. Mesenchymal stem cells: Emerging mechanisms of immunomodulation and therapy. World J Stem Cells 2014;6:526–539.

13 Traktuev DO, Merfeld-Clauss S, Li J et al. A population of multipotent CD34-positive adipose stromal cells share pericyte and mesenchymal surface markers, reside in a periendothelial location, and stabilize endothelial networks. Circ Res 2008;102:77–85.

14 Park SS. Cell therapy applications for retinal vascular diseases: Diabetic retinopathy and retinal vein occlusion. Invest Ophthalmol Vis Sci 2016;57:ORSFj1–ORSFj10.

15 Hajmousa G, Elorza AA, Nies VJ et al. Hyperglycemia induces bioenergetic changes in adipose-derived stromal cells while their pericytic function is retained. Stem Cells Dev 2016;25:1444–1453.

16 Kume T. Novel insights into the differential functions of Notch ligands in vascular formation. J Angiogenes Res 2009;1:8.

17 Sweeney C, Morrow D, Birney YA et al. Notch 1 and 3 receptor signaling modulates vascular smooth muscle cell growth, apoptosis, and migration via a CBF-1/RBP-Jk dependent pathway. FASEB J 2004;18:1421–1423.

18 Morrow D, Cullen JP, Liu W et al. Sonic Hedgehog induces Notch target gene expression in vascular smooth muscle cells via VEGF-A. Arterioscler Thromb Vasc Biol 2009;29:1112–1118.

19 Morrow D, Sweeney C, Birney YA et al. Cyclic strain inhibits Notch receptor signaling in vascular smooth muscle cells in vitro. Circ Res 2005;96:567–575.

20 Shah AV, Birdsey GM, Peghaire C et al. The endothelial transcription factor ERG mediates Angiopoietin-1-dependent control of Notch signalling and vascular stability. Nat Commun 2017;8:16002.

21 Liu H, Zhang W, Kennard S et al. Notch3 is critical for proper angiogenesis and mural cell investment. Circ Res 2010;107:860–870.

22 Liu H, Kennard S, Lilly B. NOTCH3 expression is induced in mural cells through an autoregulatory loop that requires endothelial-expressed JAGGED1. Circ Res 2009;104:466–475.

23 Hellstrom M, Phng LK, Hofmann JJ et al. Dll4 signalling through Notch1 regulates formation of tip cells during angiogenesis. Nature 2007;445:776–780.

24 Benedito R, Roca C, Sorensen I et al. The notch ligands Dll4 and Jagged1 have opposing effects on angiogenesis. Cell 2009;137:1124–1135.

25 Ahmad I, Balasubramanian S, Del Debbio CB et al. Regulation of ocular angiogenesis by Notch signaling: Implications in neovascular age-related macular degeneration. Invest Ophthalmol Vis Sci 2011;52:2868–2878.

26 Zuk PA, Zhu M, Ashjian P et al. Human adipose tissue is a source of multipotent stem cells. Mol Biol Cell 2002;13:4279–4295.

27 Banumathi E, Haribalaganesh R, Babu SS et al. High-yielding enzymatic method for isolation and culture of microvascular endothelial cells from bovine retinal blood vessels. Microvasc Res 2009;77:377–381.

28 Schneider CA, Rasband WS, Eliceiri KW. NIH Image to ImageJ: 25 years of image analysis. Nat Methods 2012;9:671–675.

29 Tanimoto N, Michalakis S, Weber BH et al. In-depth functional diagnostics of mouse models by single-flash and flicker electroretinograms without adapting background illumination. Adv Exp Med Biol 2016;854:619–625.

30 Bray SJ. Notch signalling in context. Nat Rev Mol Cell Biol 2016;17:722–735.

31 Hajmousa G, Elorza AA, Nies VJ et al. Hyperglycemia induces bioenergetic changes in adipose-derived stromal cells while their pericytic function is retained. Stem Cells Dev 2016;25:1444–1453.

32 Smith LE, Wesolowski E, McLellan A et al. Oxygen-induced retinopathy in the mouse. Invest Ophthalmol Vis Sci 1994;35:101–111.

33 Ezquer M, Urzua CA, Montecino S et al. Intravitreal administration of multipotent mesenchymal stromal cells triggers a cytoprotective microenvironment in the retina of diabetic mice. 2016;7:42.

34 Ng TK, Fortino VR, Pelaez D et al. Progress of mesenchymal stem cell therapy for neural and retinal diseases. World J Stem Cells 2014;6:111–119.

35 Benedito R, Rocha SF, Woeste M et al. Notch-dependent VEGFR3 upregulation allows angiogenesis without VEGF-VEGFR2 signalling. Nature 2012;484:110–114.

36 Lindahl P, Johansson BR, Leveen P et al. Pericyte loss and microaneurysm formation in PDGF-B-deficient mice. Science 1997;277:242–245.

37 Jo N, Mailhos C, Ju M et al. Inhibition of platelet-derived growth factor B signaling enhances the efficacy of anti-vascular endothelial growth factor therapy in multiple models of ocular neovascularization. Am J Pathol 2006;168:2036–2053.

38 Ogura S, Kurata K, Hattori Y et al. Sustained inflammation after pericyte depletion induces irreversible blood-retina barrier breakdown. JCI Insight 2017;2:e90905.

39 Rajashekhar G, Ramadan A, Abburi C et al. Regenerative therapeutic potential of adipose stromal cells in early stage diabetic retinopathy. PLoS One 2014;9:e84671.

40 Machalinska A, Kawa M, Pius-Sadowska E et al. Long-term neuroprotective effects of NT-4-engineered mesenchymal stem cells injected intravitreally in a mouse model of acute retinal injury. Invest Ophthalmol Vis Sci 2013;54:8292–8305.

41 Tzameret A, Sher I, Belkin M et al. Transplantation of human bone marrow mesenchymal stem cells as a thin subretinal layer ameliorates retinal degeneration in a rat model of retinal dystrophy. Exp Eye Res 2014;118:135–144.

42 Villacampa P, Menger KE, Abelleira L et al. Accelerated oxygen-induced retinopathy is a reliable model of ischemia-induced retinal neovascularization. PLoS One 2017;12:e0179759.

See www.StemCells.com for supporting information available online.